# Design and Performance Analysis of Millimetre-Wave Rotman Lens-Based Array Beamforming Networks for Large-Scale Antenna Subsystems

**Ardavan Rahimian**[*]**, Yasir Alfadhl, and Akram Alomainy**

**Abstract**—This paper presents the comprehensive analytical design and numerical performance evaluation of novel millimetre-wave (mm-wave) switched-beam networks, based on the Rotman lens (RL) array feeding concept. These passive array devices have been designed for operation in the 28-GHz frequency band, covering the whole 18–38 GHz frequency range. The primary objective of the work is to conduct a thorough feasibility study of designing wideband mm-wave beamformers based on liquid-crystal polymer (LCP) substrates, to be potentially employed as low-cost and high-performance subsystems for the advanced transceiver units and large-scale antennas. The presented RLs exhibit significant output behaviours for electronic beam steering, in terms of the scattering ($S$) parameters, phase characteristics, and surface current distributions, as the feeding systems' primary functionality indicators.

## 1. INTRODUCTION

Large-scale antenna systems, also known as massive multiple-input multiple-output (MIMO), and mm-wave communications are considered as the two main physical (PHY) layer key enabling techniques and promising candidate technologies, in order to address the requirements of the modern wireless communications [1–3]. These emerging systems include the fifth generation (5G) cellular networks and the associated infrastructures and subsystems, such as wireless backhaul, base station (BS), access point (AP), and user equipment (UE) units, and ultra-dense networks (UDNs) [4]. As a promising way to boost the capacity, these technologies employ bandwidths with multiple GHz, and therefore convey very high data rates to improve the capacity, to deliver multi-Gbps transmission, and to meet the demands for exploit of large bandwidth and higher spectral efficiency, required for the future wireless systems [5].

However, radiowave propagation in the mm-wave bands of the electromagnetic (EM) spectrum suffers from a number of severe losses that result in the link quality degradation and wireless channel impairment, due to the shorter wavelengths than the conventional sub-6 GHz microwave systems [6]. These path loss components mainly include the atmospheric oxygen absorption, water vapour absorption, rain and foliage attenuations, blockage effects, and penetration, reflection, diffraction, and scattering losses. Although this attenuation facilitates the spatial frequency reuse in the UDN small cells in both the line-of-sight (LoS) and non-line-of-sight (NLoS) channel conditions, as part of the intended radio frequency (RF) architecture and system development framework, it necessitates the conduct of a thorough RF link budget analysis (LBA). Therefore, this would improve the overall service coverage, enhance reliable communication performance, and provide guaranteed scalable quality of service (QoS) solutions to the UEs [7].

In view of this, array beamforming networks (BFNs), as one of the crucial techniques to efficiently mitigate the high propagation path loss in the frequency bands, are used to effectively create narrow beams with significant gains, and to accommodate directional system transmission required for the antenna arrays, as integrated subsystems of the large-scale transceivers. These RF beamformers further allow for the appropriate provision of a number of distinctive features, such as maintaining the acceptable signal-to-noise ratio (SNR), providing the high precoding gains and sufficient signal power, improving the spectral efficiency (i.e., by enabling multiple data streams), and extending the RF transmission range. Also, thanks to the small wavelengths of mm-wave bands a large number of antenna elements can be integrated within a relatively compact physical dimensions at both the transmitter and receiver of the wireless transceivers in the mm-wave communication systems. This leads to synthesising highly directional beams, resulting in high beamforming gains with low interference, and therefore realising the intended wireless subsystem based on the essential conduct of the LBA.

In this regard, for the purpose of appropriately exploiting the multiplexing gains and supporting the data stream transmission, as well as controlling the RF signal phase at each element of the antenna array, a single mm-wave beamformer is connected to multiple antennas, which applies complex coefficients to fully utilise the RF signals to compensate for the path loss at the intended frequency bands [8, 9]. This further provides the phased array system with the baseband signal per RF chain in which an extra radio at each port of the MIMO system can be integrated for the RF-digital signal processing to efficiently mitigate inter-user interference (IUI), and to potentially optimise the capacity of the wireless communication system using various hybrid beamforming techniques [10, 11].

Therefore, the mm-wave multibeam antenna array systems are then fed by the passive BFNs, as the core components that perform the electronic beam steering. Several RF beamforming techniques using different architectures are reported in the literature, based on the circuit-based BFNs, such as the Blass matrix, Butler matrix, Nolen matrix, and coherently radiating periodic structures (CORPS) [12–16], as well as the lens-based and innovative RF beamforming methods [17–21]. This investigation is of vital importance to thoroughly take into account the systematic wireless design framework for the potential RF integration at the large-scale levels.

The remainder of this paper is organised as follows. Section 2 presents the theoretical design and analysis of the RL devices with different configurations, based on the constituent equations. In Section 3, the proposed wideband mm-wave beamformer, along with the evaluation of the output performances, is presented. Section 4 presents the developed large-scale RLs, along with the analysis of the characteristics, i.e., to the best of the authors' knowledge, this is the first attempt in order to design the LCP-based large-scale mm-wave Rotman lens-based array beamforming networks. The paper is concluded in Section 5.

## 2. THEORETICAL DESIGN AND ANALYSIS

The Rotman lens-based BFN enables multibeam phased array systems to generate scanning beams for the reliable electronic beam steering. This switched-beam passive network is properly designed in order to provide the array with the correct phase and acceptable amplitude distributions across the aperture [22]. The low-profile RL is capable of focusing the energy into a geometrically-configured cavity, in order to appropriately produce a wave-front across the output that is phased by the time-delay in the RF signal transmission, and to scan a beam in the desired pattern that radiates a circular phase-front within the lens cavity [23]. The theoretical formulations have been modified and improved over the years, based on the rigorous equations derived from the geometrical optics (GO) [24–26]. The design of the trifocal lens-based beamformer with the homogeneous medium is controlled by a series of equations that set the focal points, array positions, and lengths of transmission lines, in order to provide the antenna array with the beam patterns that can be effectively steered in certain directions, along with suppressing the undesired ones [27–29]. The RL design and synthesis procedure ensures the parameters to be tuned to effectively optimise the network performance, in terms of phase and amplitude errors, reflection and transmission coefficients, and sidelobe levels (SLLs) [30–32]. The intention of this section is to briefly explain the fundamental operation of the trifocal RLs, and then continuing onto the presentation of the developed mm-wave lens-based beamformers.

Figure 1 shows a schematic diagram of a trifocal RL [33] with input (i.e., beam contour) and

output (i.e., array contour) ports lie on either side of the cavity (i.e., an etched thin copper layer on the dielectric substrate). It incorporates three theoretically perfect focal points (i.e., no path length errors), namely $F_1$, $F_2$, and $F_0$, in which the latter is located on the central axis (i.e., on-axis focal point), while the other two are symmetrically located on the circular focal arc at $\pm\alpha$ (i.e., off-axis focal points). For all other points, the phase errors occur, since the path length will not be a linear function of the input beam position. At the wave-front, all the rays must be in phase independent of the path they travel. The coordinates of two off-axis focal points $F_1$ and $F_2$ and one on-axis focal point $F_0$ are $(-F\cos(\alpha),\, F\sin(\alpha))$, $(-F\cos(\alpha),\, -F\sin(\alpha))$, and $(-G, 0)$, respectively [34]. $\text{TL}_0$ and TL are the microstrip transmission lines (MTLs), with lengths denoted by $W_0$ and $W$, respectively; $\theta$ is also defined as the radiation angle corresponding to the focal points. The relative permittivity factors for the cavity and radiation environment are given as $\varepsilon_r$ and $\varepsilon_i$, respectively. The MTLs, with the effective dielectric constant of $\varepsilon_e$, are routed with the appropriate curvature in order to guarantee the separation and non-overlapping required for the array contour, and also to maintain the same electrical length among all the output meandered MTLs. In the generalised RL model, it is assumed that the focal angle $\alpha$ is equal to the scan angle $\theta$, and although the angles can be different, by applying which, it can be used for the potential computations and optimisations regarding the compactness of the beam region and phase error reductions [35].
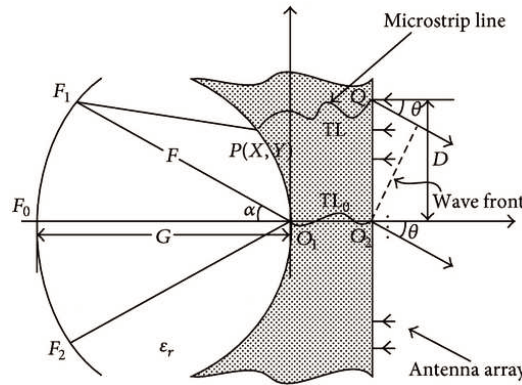


**Figure 1.** Configuration and design parameters of the microstrip trifocal Rotman lens-based array beamformer.

The following equations govern the design of the trifocal RL based on the GO, in order to maintain the performance of the device, in terms of generating multiple beams with a linear progressive phase shift across the array ports (i.e., due to the different electrical lengths between a specific beam port and all output ports), as well as preventing the array from changing the scanning direction with frequency variation, i.e., the high-performance wideband true-time-delay (TTD) operation of the microwave/mm-wave lens. Hence, the TTD-based beamformer, provides the linear phase progression on the array ports based on maintaining a constant time-delay over a wide frequency range of operation. In the RL design procedure, the main governing equations impose the condition of path equality based on the ray tracing model, in order to derive the lens geometry. The equations also address methods of explicitly solving for the geometry of the receiver contour, i.e., $P(X, Y)$; which is defined by the position of the three focal points, as well as the width of the output array contour (i.e., $2D$); and $W$, as the primary parameters that enable the array to scan into a certain known direction [36].

$$(\overrightarrow{F_1 P})\sqrt{\varepsilon_r} + W\sqrt{\varepsilon_e} + D\sqrt{\varepsilon_i}\sin(\theta) = F\sqrt{\varepsilon_r} + W_0\sqrt{\varepsilon_e}; \tag{1}$$

$$(\overrightarrow{F_2 P})\sqrt{\varepsilon_r} + W\sqrt{\varepsilon_e} - D\sqrt{\varepsilon_i}\sin(\theta) = F\sqrt{\varepsilon_r} + W_0\sqrt{\varepsilon_e}; \tag{2}$$

$$(\overrightarrow{F_0 P})\sqrt{\varepsilon_r} + W\sqrt{\varepsilon_e} = G\sqrt{\varepsilon_r} + W_0\sqrt{\varepsilon_e}. \tag{3}$$

The design equations provide the method for thoroughly designing the mm-wave beamformers shown in Fig. 2, in order to operate in the 18–38 GHz band, with the switched-beam scanning coverage of $\pm30°$. The lens-based networks are developed based on the Rogers ULTRALAM 3850HT flexible,
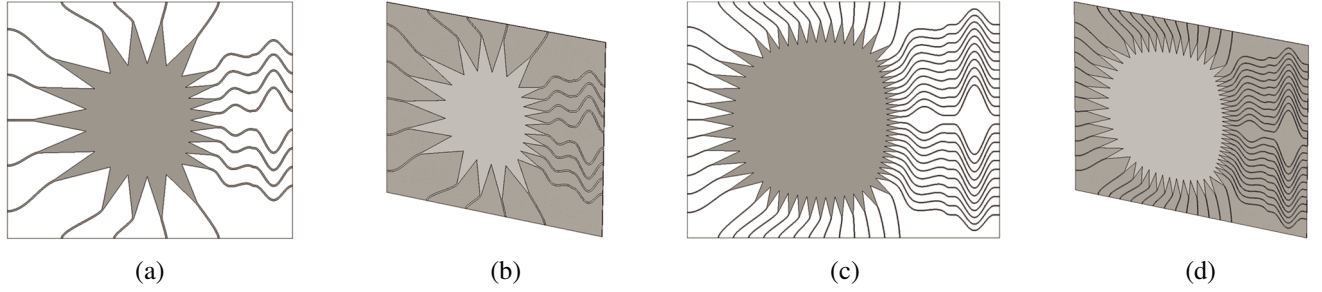
**Figure 2.** Simulated planar Rotman lenses: (a) wideband mm-wave beamformer with 5 beam ports, 8 array ports, and 8 dummy ports, with dimensions of $67.45 \times 81.87\,\mathrm{mm}^2$, front view; (b) perspective view; (c) large-scale mm-wave beamformer with 11 beam ports, 22 array ports, and 26 dummy ports, with dimensions of $139.97 \times 185.86\,\mathrm{mm}^2$, front view; (d) perspective view.

recyclable, and multi-environmental LCP laminates, with the dielectric constant of $\varepsilon_r = 2.9$, loss tangent of $\tan\delta = 0.0025$, substrate thickness of $h = 0.18\,\mathrm{mm}$, and top- and bottom-cladding of $t = 17.5\,\mathrm{\mu m}$, as in [37–41], with the port-pointing enabled; i.e., the beam and array ports are adjusted so that the boresight of each taper points to the centre of the opposite contour, rather than being normal to the lens surface; in order to enhance the performance of the proposed Rotman lenses.

## 3. WIDEBAND MILLIMETRE-WAVE ROTMAN LENS-BASED BEAMFORMER

### 3.1. Wideband Rotman Lens-Based BFN: Scattering Parameters

The high-performance computing (HPC)-based full-wave high-resolution simulations have been conducted, based on deploying the finite integration technique (FIT) using the robust transient solver; i.e., discretisation of the integral form of Maxwell's equations [42, 43]; to rigorously evaluate the time-domain characteristics of the electrically-large BFNs. Fig. 3 shows the characteristics of the dummy ports as an integral part of the lens, over the frequency range of operation, which are terminated with 50-$\Omega$ matched loads. The sidewall contours along with the dummy ports are efficiently designed and implemented to minimise the multiple reflections and standing waves from the sidewalls, which consequently results in the improved performance, in terms of the device efficiency [40, 44]. Fig. 3 depicts the primary contribution levels of the match-terminated dummy ports, denoted by the elements 1 to 8, for the excited beam ports 1 and 3, corresponding to the exertions of the minimum and maximum device efficiencies, respectively. Dummy port 1 is located adjacent to beam port 1, and progressively, dummy port 8 is located adjacent to array port 13. The graphical representations in the subsequent sections will show the impact of these dummy ports on the overall EM-centric behaviour of the RF lenses.
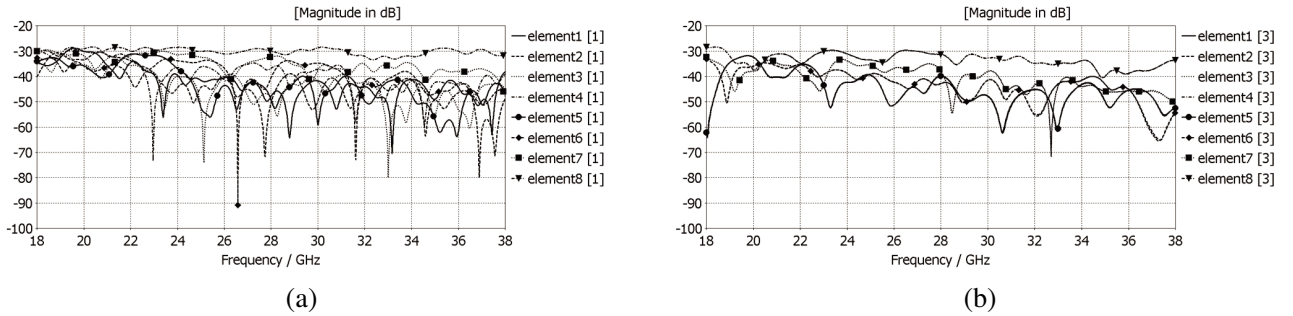


**Figure 3.** Simulated lumped element current plots of the dummy ports (i.e., element-1 to element-8) of the LCP-based wideband mm-wave RL beamformer: (a) magnitude plots for input beam port 1 active; (b) magnitude plots for input beam port 3 active.

Figures 4(a) to (c) present the transmission coefficients of the proposed lens for the excited input beam ports 1 to 3, respectively. As the $S$-parameters clearly depict, the mm-wave RL exhibits the desired wideband characteristics across the whole frequency range, and further maintains an almost uniform power distribution through the RL cavity, based on the behavioural conformity according to the generalised trifocal lens theory. The isolation characteristics among the input beam ports have been analysed, in order to confirm the significant operation of the device, in terms of providing the required isolations among the input ports to retain the performance of the BFN for the efficient operation in the whole frequency range. It should be noted that the overall distribution behaviour of input beam ports 1 and 2 are theoretically identical to the output characteristics of input beam ports 5 and 4, respectively, due to the intrinsic symmetrical structure of the RL. The device efficiency at the centre frequency of 28-GHz is also numerically computed as 45.1%. Fig. 4(d) depicts the reflection coefficient plots for the activated ports 1 to 5, which also confirms the wideband maintenance.

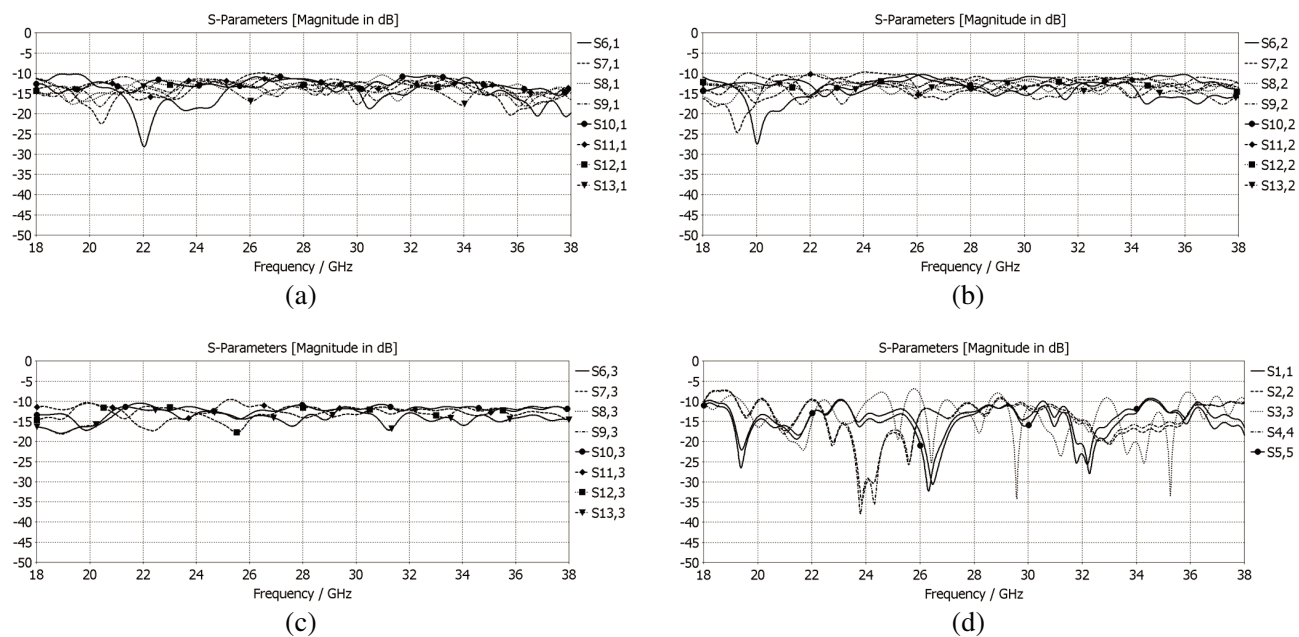Figures 5(a) and (b) present the output phase characteristics of the mm-wave beamformer across



**Figure 4.** Simulated $S$-parameters of the planar LCP-based 28-GHz $5 \times 8$ Rotman lens beamformer for the wideband operation: (a) transmission coefficient plots for input beam port 1 active; (b) transmission coefficient plots for input beam port 2 active; (c) transmission coefficient plots for input beam port 3 active; (d) reflection coefficient plots for input beam ports 1 to 5 active.
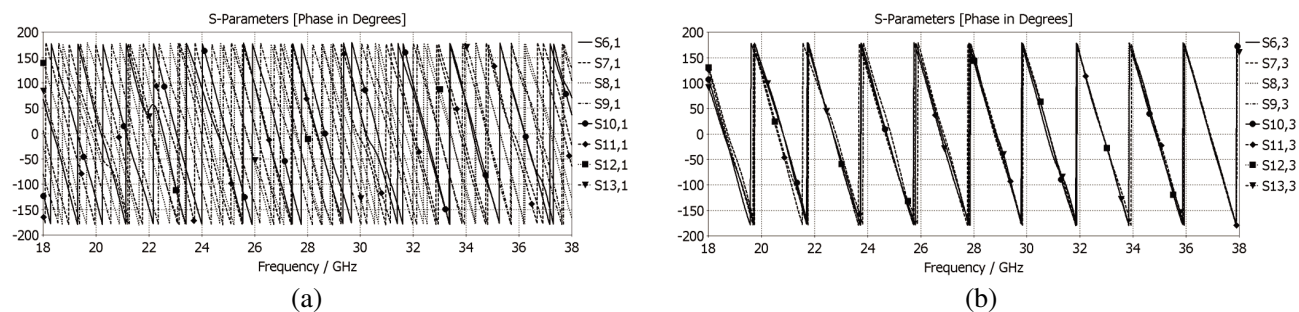


**Figure 5.** Simulated $S$-parameters of the planar LCP-based 28-GHz $5 \times 8$ Rotman lens beamformer for the wideband operation: (a) linear phase distributions for input beam port 1 active; (b) linear phase distributions for central input beam port 3 active.

the entire operating bandwidth of 18–38 GHz, when input beam ports 1 and 3 are fed, respectively. It can be noticed that the lens exhibits outstanding performance for the electronic beam steering, in terms of the required constant phase difference as a function of frequency, as well as the linear phase distributions. The maximum EM power is delivered to the output ports, and the progressive amplitude and phase distributions further confirm the high-performance operation of the mm-wave lens. The RL conducts the distribution of the energy across the array ports, hence resulting in the provision of the RF beam scanning to be effectively deployed for the wireless communication subsystems.

## 3.2. Wideband Rotman Lens-Based BFN: Surface Current Distributions

Figures 6(a) to (e) present the computed surface current distributions of the RL, when beam ports 1 to 5 are fed, respectively. The figures depict the progressive distributions of the EM energy across the array ports, as well as the intensities of the power throughout the RF device. Fig. 6(f) indicates the lens with the deployed EM range, i.e., the same scale for the other configurations, as well.
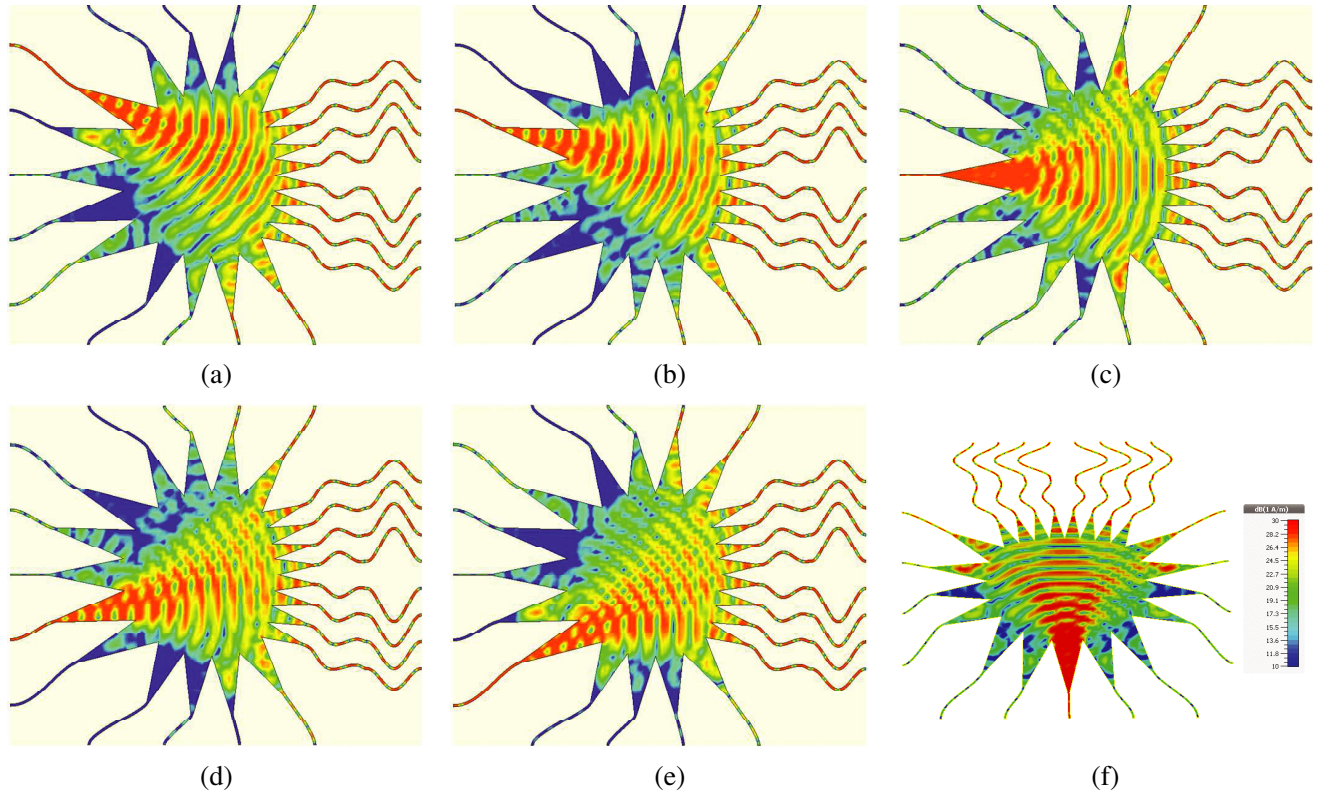


(a)                                         (b)                                         (c)

(d)                                         (e)                                         (f)

**Figure 6.** Surface current distributions of the LCP-based wideband $5 \times 8$ Rotman lens RF beamformer, for the excited beam ports at centre frequency $f = 28$-GHz: (a) input beam port 1 active; (b) input beam port 2 active; (c) input beam port 3 active; (d) input beam port 4 active; (e) input beam port 5 active; (f) RL device core with beam port 3 active, along with the deployed EM scale.

## 4. LARGE-SCALE MILLIMETRE-WAVE ROTMAN LENS-BASED BEAMFORMER

### 4.1. Large-Scale Rotman Lens-Based BFN: Scattering Parameters

The constituent equations of the trifocal lens-based beamformers have been effectively utilised, in order to undertake the design of the extended RF structures based on the presented LCP-based mm-wave RL. This section shows the conducted high-performance simulations regarding the comprehensive representation of the output characteristics of the developed RLs, designed specifically to serve as
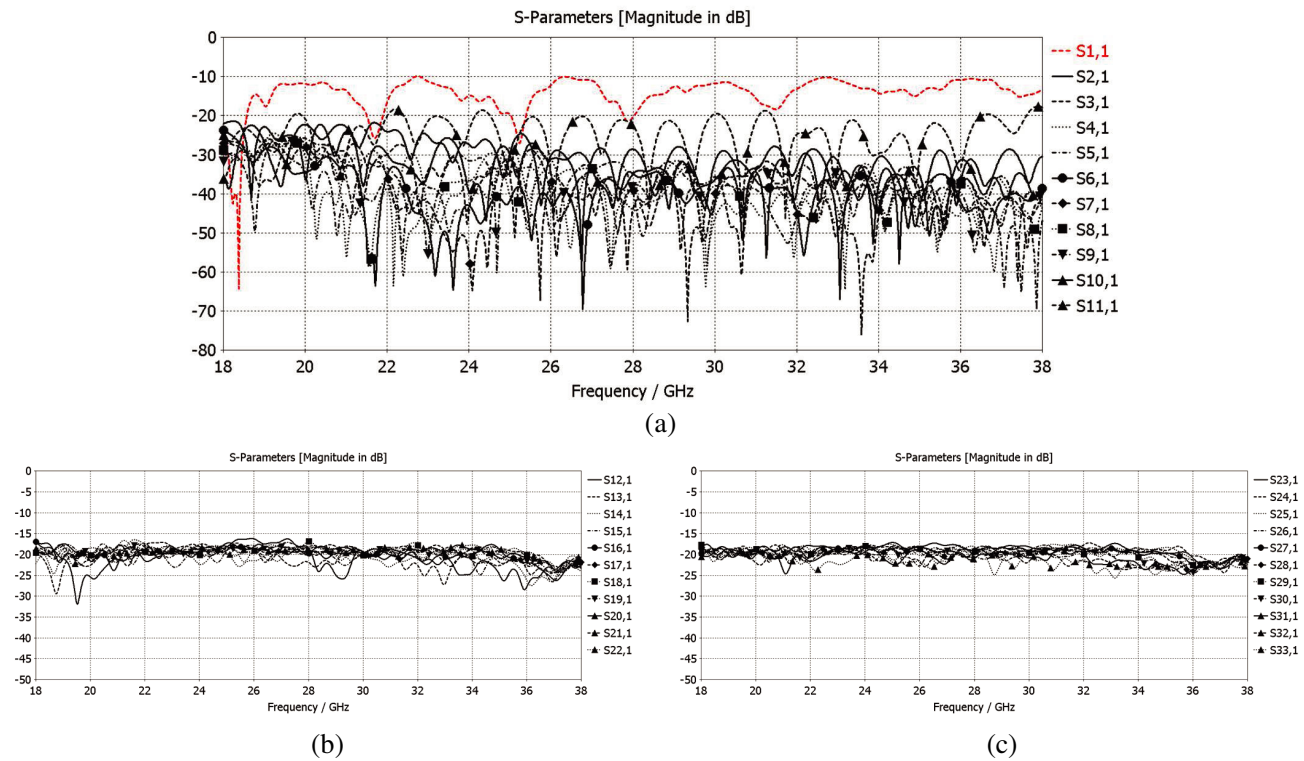
**Figure 7.** Simulated *S*-parameters: (a) reflection coefficient and isolation plots for port 1 active; (b) transmission coefficient plots for port 1 active, Set I (i.e., ports 12 to 22); (c) transmission coefficient plots for port 1 active, Set II (i.e., ports 23 to 33).

efficient passive feeding networks for the large-scale antenna subsystems, as part of the advanced wireless infrastructures.

Figures 7(a) and 8(a) present the reflection coefficient and isolation plots for the excited ports 1 and 6, respectively. The output results depict the desired behaviour of the planar LCP-based large-scale lens-based BFN, in terms of maintaining the distributed EM power levels over the whole frequency range of operation. Moreover, Figs. 7(b) and (c) and Figs. 8(b) and (c) present the transmission coefficients for the activated beam ports 1 and 6, respectively. As it can be observed from the comprehensive full-wave EM results, the large-scale feeding system exhibits linear distributions of power with low-ripple characteristics, across the operating frequency range of 18–38 GHz, over the whole set of array ports 12 to 33 (i.e., 22 output ports), hence confirming the wideband operation of the lens. This originally exploited RF characteristics of the developed large-scale RL, can be effectively utilised in the massive MIMO systems for the future wireless architectures, in order to overcome the imperfect ambient conditions in the mm-wave channels.

Moreover, Figs. 9(a) and (b) extensively illustrate the output phase division behaviour of the large-scale lens-based beamformer, when the beam ports 1 and 6 are excited, respectively. It is worth noting that input ports 1 and 6 determine the minimum and maximum device efficiency boundaries, since they are placed on the furthest distance from the central focal point of the lens, as well as on the central axis of the RL, respectively [40]. The computed device efficiency at the centre frequency of 28-GHz is also obtained as 26.5%. The presented plots indicate the linear phase distributions across the output array ports of the large-scale RL; i.e., depicted in two different sets for beam ports 1 and 6, for a clear representation; hence, substantially meeting the primary requirements of the electronic beam steering, for the efficient deployment of the mm-wave subsystems. The proposed large-scale lens-based BFN can be potentially employed as a powerful core of the communication system, in a number of intelligent wireless applications. The lens is able to provide the system with the essential beam steering capabilities, in the scenarios where the appropriate implementation of a large number of antennas and subsystems
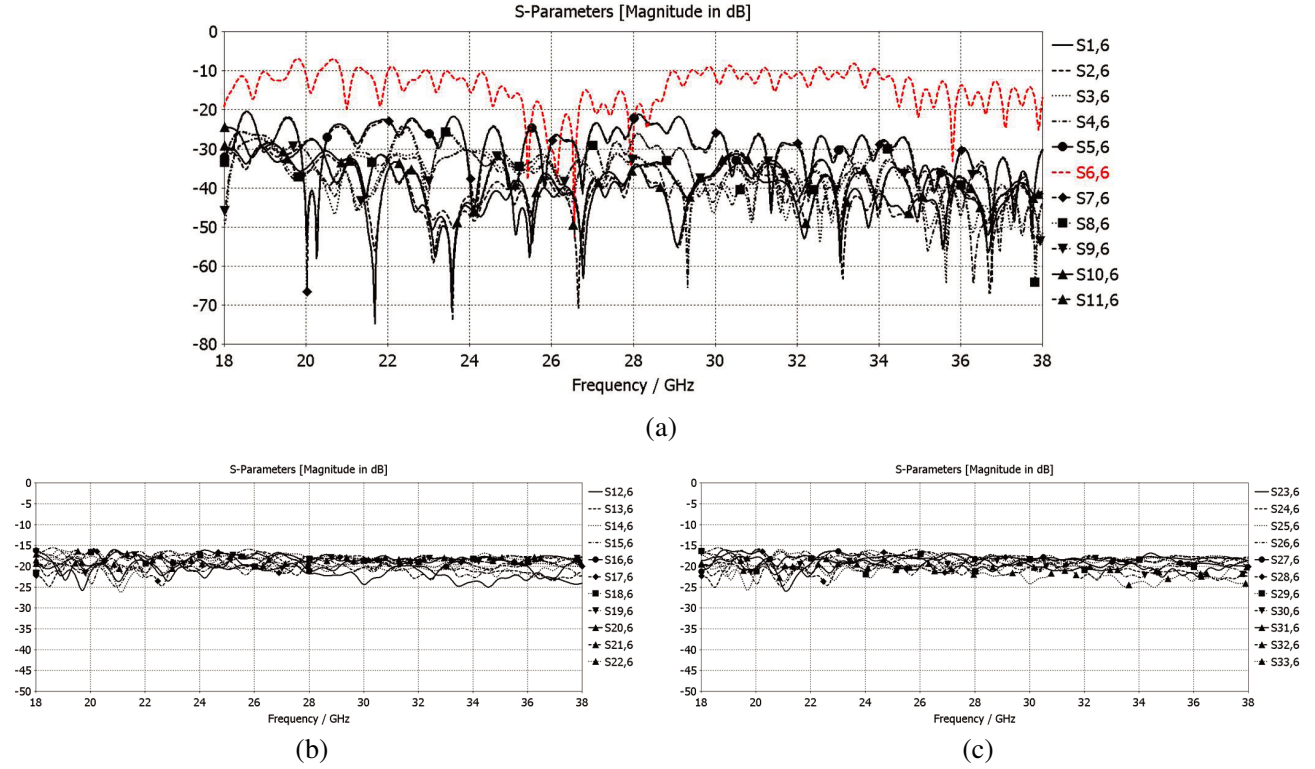
(a)



(b)                                                                    (c)

**Figure 8.** Simulated *S*-parameters: (a) reflection coefficient and isolation plots for port 6 active; (b) transmission coefficient plots for port 6 active, Set I (i.e., ports 12 to 22); (c) transmission coefficient plots for port 6 active, Set II (i.e., ports 23 to 33).
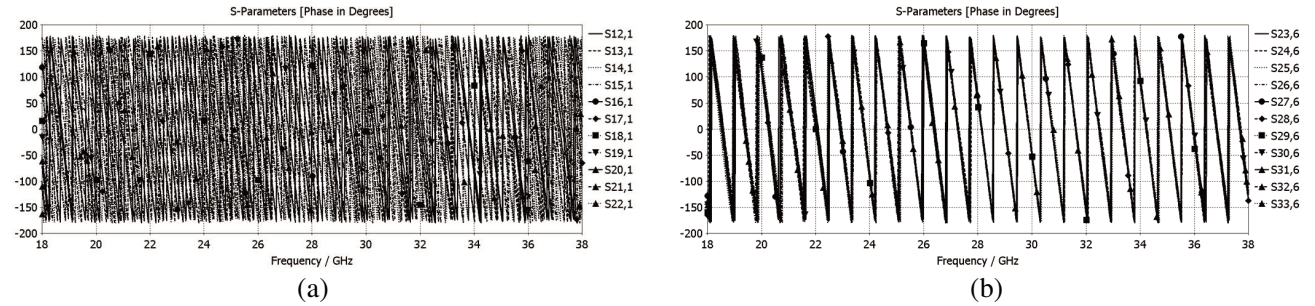


(a)                                                                    (b)

**Figure 9.** Simulated *S*-parameters of the planar LCP-based 28-GHz 11 × 22 Rotman lens beamformer for the wideband operation: (a) linear phase distributions for input beam port 1 active, Set I (i.e., output array ports 12 to 22); (b) linear phase distributions for central input beam port 6 active, Set II (i.e., output array ports 23 to 33).

based on the digital beamforming methods, as well as the circuit-based beamforming systems with higher device efficiencies, is enormously complex, costly, power consuming, lossy, bulky, and inflexible.

## 4.2. Large-Scale Rotman Lens-Based BFN: Surface Current Distributions

Figures 10(a) to (f) present the surface current distributions of the planar LCP-based large-scale lens-based beamformer at the centre frequency, for the activated input beam ports 1 to 6, respectively. This high-resolution full-wave representation clearly illustrates the behaviour of the EM wave while travelling within the lens cavity, starting from the excited beam ports, then across the electrically-large structure,
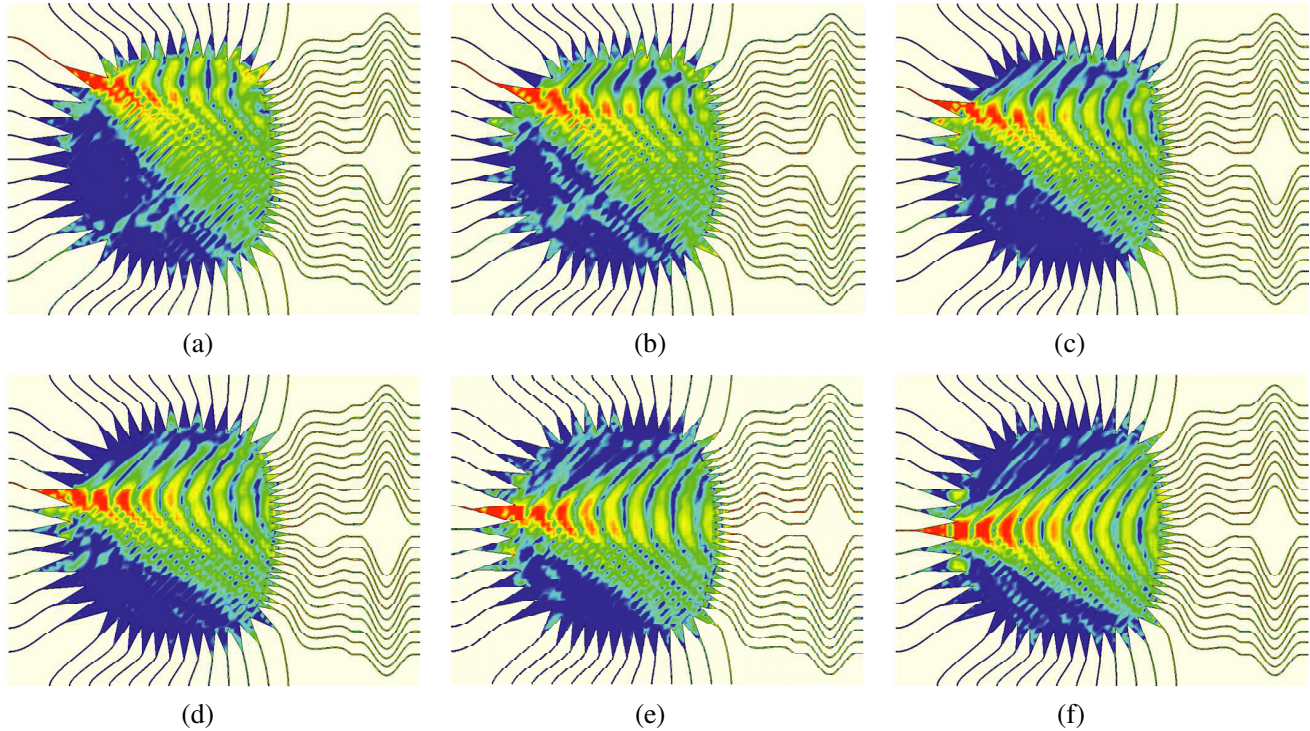
**Figure 10.** Surface current distributions of the LCP-based large-scale $11 \times 22$ Rotman lens RF beamformer, for the excited beam ports at centre frequency $f = 28$-GHz: (a) input beam port 1 active; (b) input beam port 2 active; (c) input beam port 3 active; (d) input beam port 4 active; (e) input beam port 5 active; (f) central input beam port 6 active.

and further over the array contour, in order to efficiently distribute the EM energy among the output array ports.

## 4.3. Large-Scale Rotman Lens-Based BFN: 32- and 64-Element Feeding Systems

The presented high-performance LCP-based $11 \times 22$ RL beamformer has been extended into two other large-scale RF structures, as shown in Figs. 11(a) and (b), in order to appropriately feed 32- and 64-element phased array systems, respectively. The BFNs have been developed based on the original trifocal constituent equations, which are effectively used to design the LCP-based RLs. The inherent mechanism of these lens-based BFNs to appropriately perform the beam scanning, is also based on equalising the electrical path from an input beam port to an output port across the large-scale array contour, with the time-delay of the corresponding planar wave-front from a given far-field direction, consequently resulting in the generation of an RF beam in the corresponding direction.

In order to efficiently deploy the intelligent wireless communications, the advanced RF beamformers, as the dominant component of most multibeam antenna systems, as well as the core of the hybrid networks, are able to significantly improve the performance of the mm-wave transceiver systems, through maintaining the consistent RF characteristics, improving the throughput and data rate of the system, and accommodating the directional transmissions. As thoroughly presented in this work, these compact and lightweight lens-based beamformers offer cost-effective solutions for the communication scenarios in which a large number of antenna elements are of crucial importance in order to steer the direction of the main lobe of the radiation, to compensate the path loss, and to realise the reliable RF communication links; i.e., currently implemented based on the costly and high power consumption methods using the conventional MIMO systems with separate chains and digital units, along with complex signal processing. Hence, the proposed BFNs precisely enable the desired distributions of amplitude and phase coefficients, in order to properly excite a corresponding number of array elements for the potential
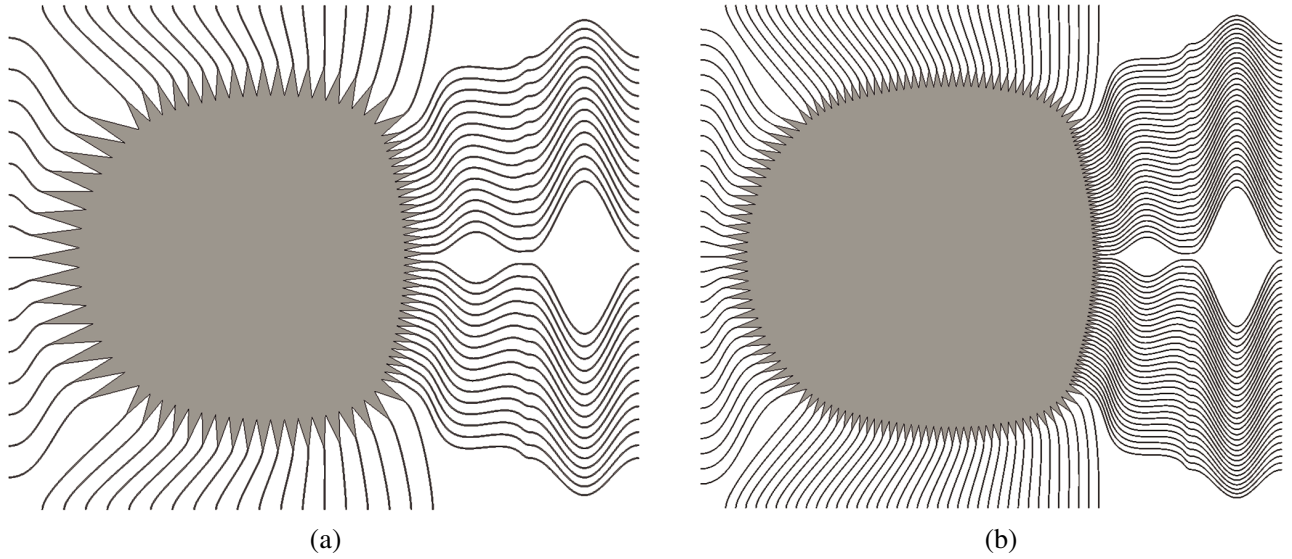
(a)                                                                          (b)

**Figure 11.** Simulated planar LCP-based large-scale 28-GHz Rotman lens array beamforming networks: (a) RF beamformer with 15 beam ports, 32 array ports, and 38 dummy ports, with dimensions of $208.49 \times 261.20\,\mathrm{mm}^2$; (b) RF beamformer with 31 beam ports, 64 array ports, and 76 dummy ports, with dimensions of $398.23 \times 460.64\,\mathrm{mm}^2$.

electronically steerable beamforming, thereby facilitating a higher effective isotropic radiated power (EIRP) in the transmit mode, as well as an improved SNR in the receive mode, as part of the wireless transceiver implementation.

## 5. CONCLUDING REMARKS

This contribution has comprehensively undertaken the analytical design and performance evaluations of the mm-wave wideband and large-scale Rotman lens-based array beamforming networks, based on the rigorous high-resolution computational full-wave EM simulations using the CST STUDIO SUITE software. The presented results confirm the high-performance operation of the mm-wave BFNs, in terms of exhibiting significant output characteristics, including the linear and low-ripple amplitude distributions across the output ports, progressive phase division among the array ports, wideband operation of the RLs with the minimised phase error, and efficient surface current distributions over the array contours. The developed Rotman lens-based RF beamformers, include the LCP-based $5 \times 8$, $11 \times 22$, $15 \times 32$, and $31 \times 64$ array feeding networks, specifically realised based on the original trifocal constituent design equations, and further optimised in terms of the lens parameters' intrinsic functionalities. Hence, the mm-wave BFNs provide the advanced large-scale antenna systems with the low-profile and high-performance wireless subsystems capable of electronic beam steering, required for the efficient deployment and utilisation of the next-generation telecommunication systems and services.

The presented investigation can be further extended into the performance evaluations of the designed 32- and 64-element array feeding networks, as conducted for the 22-element large-scale array beamformer. The LCP-based RLs have also remarkable potential to be deployed in the conformal wireless subsystems. Therefore, the thorough RF performance analysis can also be extended into the case of introducing the proposed flexures in [40], into the structures of the developed 28-GHz wideband and large-scale RLs. This would lead to the appropriate feasibility study of implementing such flexible large-scale Rotman lens-based beamformers according to the aerodynamic and hydrodynamic properties of the bearing surfaces, as well as the configurations of the intended wireless system infrastructures. Hence, the core of the conducted design and performance analysis can be considered as a comprehensive generalised design framework for the optimal analytical evaluations of array beamforming networks, for a variety of RF and wireless applications.

## REFERENCES

1. Kutty, S. and D. Sen, "Beamforming for millimeter wave communications: An inclusive survey," *IEEE Communications Surveys & Tutorials*, Vol. 18, No. 2, 949–973, 2016.

2. Pang, X., W. Hong, T. Yang, and L. Li, "Design and implementation of an active multibeam antenna system with 64 RF channels and 256 antenna elements for massive MIMO application in 5G wireless communications," *China Communications*, Vol. 11, No. 11, 16–23, Nov. 2014.

3. Yuan, H.-W., G.-F. Cui, and J. Fan, "A method for analyzing broadcast beamforming of massive MIMO antenna array," *Progress In Electromagnetics Research Letters*, Vol. 65, 15–21, 2017.

4. Agiwal, M., A. Roy, and N. Saxena, "Next generation 5G wireless networks: A comprehensive survey," *IEEE Communications Surveys & Tutorials*, Vol. 18, No. 3, 1617–1655, 2016.

5. Ala-Laurinaho, J., et al., "2-D beam-steerable integrated lens antenna system for 5G *E*-band access and backhaul," *IEEE Transactions on Microwave Theory and Techniques*, Vol. 64, No. 7, 2244–2255, Jul. 2016.

6. Uchendu, I. and J. Kelly, "Survey of beam steering techniques available for millimeter wave applications," *Progress In Electromagnetics Research B*, Vol. 68, 35–54, 2016.

7. Rahimian, A. and F. Mehran, "RF link budget analysis in urban propagation microcell environment for mobile radio communication systems link planning," *International Conference on Wireless Communications and Signal Processing (WCSP)*, 1–5, Nov. 2011.

8. Venkateswaran, V., F. Pivit, and L. Guan, "Hybrid RF and digital beamformer for cellular networks: Algorithms, microwave architectures, and measurements," *IEEE Transactions on Microwave Theory and Techniques*, Vol. 64, No. 7, 2226–2243, Jul. 2016.

9. Gao, Y., M. Khaliel, and T. Kaiser, "Wideband hybrid analog-digital beamforming massive MIMO systems based on Rotman lens," *IEEE International Conference on Communication Systems (ICCS)*, 1–6, Dec. 2016.

10. Jang, J., et al., "Smart small cell with hybrid beamforming for 5G: Theoretical feasibility and prototype results," *IEEE Wireless Communications*, Vol. 23, No. 6, 124–131, Dec. 2016.

11. Payami, S., M. Ghoraishi, and M. Dianati, "Hybrid beamforming for large antenna arrays with phase shifter selection," *IEEE Transactions on Wireless Communications*, Vol. 15, No. 11, 7258–7271, Nov. 2016.

12. Hall, P. S. and S. J. Vetterlein, "Review of radio frequency beamforming techniques for scanned and multiple beam antennas," *IEE Microwaves, Antennas and Propagation*, Vol. 137, No. 5, 293–303, Oct. 1990.

13. Fonseca, N. J. G., A. Ali, and H. Aubert, "Cancellation of beam squint with frequency in serial beamforming network-fed linear array antennas," *IEEE Antennas and Propagation Magazine*, Vol. 54, No. 1, 32–39, Feb. 2012.

14. Rahimian, A., "Investigation of Nolen matrix beamformer usability for capacity analysis in wireless MIMO systems," *19th Asia-Pacific Conference on Communications (APCC)*, 622–623, Aug. 2013.

15. Patterson, C. E., et al., "A 60-GHz active receiving switched-beam antenna array with integrated Butler matrix and GaAs amplifiers," *IEEE Transactions on Microwave Theory and Techniques*, Vol. 60, No. 11, 3599–3607, Nov. 2012.

16. Panduro, M. A. and C. del Rio-Bocio, "Design of beam-forming networks for scannable multi-beam antenna arrays using CORPS," *Progress In Electromagnetics Research*, Vol. 84, 173–188, 2008.

17. Chan, K. K. and S. K. Rao, "Design of a Rotman lens feed network to generate a hexagonal lattice of multiple beams," *IEEE Transactions on Antennas and Propagation*, Vol. 50, No. 8, 1099–1108, Aug. 2002.

18. Kushwah, R. P. S., P. K. Singhal, and P. C. Sharma, "Design of symmetric bootlace lens with gain analysis at UHF band," *Progress In Electromagnetics Research Letters*, Vol. 6, 83–89, 2009.

19. Lee, W., et al., "Beamforming lens antenna on a high resistivity silicon wafer for 60 GHz WPAN," *IEEE Transactions on Antennas and Propagation*, Vol. 58, No. 3, 706–713, Mar. 2010.

20. Lee, W., et al., "Compact two-layer Rotman lens-fed microstrip antenna array at 24 GHz," *IEEE Transactions on Antennas and Propagation*, Vol. 59, No. 2, 460–466, Feb. 2011.

21. Rahimian, A., "Microwave beamforming networks employing Rotman lenses and cascaded Butler matrices for automotive communications beam scanning electronically steered arrays," *Microwaves, Radar and Remote Sensing Symposium (MRRS)*, 351–354, Aug. 2011.

22. Rotman, W. and R. F. Turner, "Wide-angle microwave lens for line source applications," *IEEE Transactions on Antennas and Propagation*, Vol. 11, No. 6, 623–632, Nov. 1963.

23. Peterson, A. F. and E. O. Rausch, "Scattering matrix integral equation analysis for the design of a waveguide Rotman lens," *IEEE Transactions on Antennas and Propagation*, Vol. 47, No. 5, 870–878, May 1999.

24. Katagi, T., S. Mano, and S. Sato, "An improved design method of Rotman lens antennas," *IEEE Transactions on Antennas and Propagation*, Vol. 32, No. 5, 524–527, May 1984.

25. Hansen, R. C., "Design trades for Rotman lenses," *IEEE Transactions on Antennas and Propagation*, Vol. 39, No. 4, 464–472, Apr. 1991.

26. Singhal, P. K., P. C. Sharma, and R. D. Gupta, "Rotman lens with equal height of array and feed contours," *IEEE Transactions on Antennas and Propagation*, Vol. 51, No. 8, 2048–2056, Aug. 2003.

27. Simon, P. S., "Analysis and synthesis of Rotman lenses," *22nd AIAA International Communications Satellite Systems Conference & Exhibit*, 1–11, May 2004.

28. Cheng, Y. J., et al., "Substrate integrated waveguide (SIW) Rotman lens and its Ka-band multibeam array antenna applications," *IEEE Transactions on Antennas and Propagation*, Vol. 56, No. 8, 2504–2513, Aug. 2008.

29. Vashist, S., M. K. Soni, and P. K. Singhal, "A review on the development of Rotman lens antenna," *Chinese Journal of Engineering*, Vol. 2014, 1–9, article ID: 385385, Jul. 2014.

30. Christie, S., et al., "Rotman lens-based retrodirective array," *IEEE Transactions on Antennas and Propagation*, Vol. 60, No. 3, 1343–1351, Mar. 2012.

31. Tekkouk, K., M. Ettorre, L. Le Coq, and R. Sauleau, "Multibeam SIW slotted waveguide antenna system fed by a compact dual-layer Rotman lens," *IEEE Transactions on Antennas and Propagation*, Vol. 64, No. 2, 504–514, Feb. 2016.

32. Attaran, A., R. Rashidzadeh, and A. Kouki, "60 GHz low phase error Rotman lens combined with wideband microstrip antenna array using LTCC technology," *IEEE Transactions on Antennas and Propagation*, Vol. 64, No. 12, 5172–5180, Dec. 2016.

33. Wang, Z., B. Xiang, and F. Yang, "A multibeam antenna array based on printed Rotman lens," *International Journal of Antennas and Propagation*, 1–6, article ID: 179327, 2013.

34. Rahimian, A., "Design and performance of a Ku-band Rotman lens beamforming network for satellite systems," *Progress In Electromagnetics Research M*, Vol. 28, 41–55, 2013.

35. Rajabalian, M. and B. Zakeri, "Optimisation and implementation for a non-focal Rotman lens design," *IET Microwaves, Antennas & Propagation*, Vol. 9, No. 9, 982–987, Jun. 2015.

36. Dong, J. and A. I. Zaghloul, "Extremely high-frequency beam steerable lens-fed antenna for vehicular sensor applications," *IET Microwaves, Antennas & Propagation*, Vol. 4, No. 10, 1549–1558, Oct. 2010.

37. Saily, J., et al., "Millimetre-wave beam-switching Rotman lens antenna designs on multi-layered LCP substrates," *10th European Conference on Antennas and Propagation (EuCAP)*, 1–5, Apr. 2016.

38. Lamminen, A., et al., "Gain enhanced millimetre-wave beam-switching Rotman lens antenna designs on LCP," *11th European Conference on Antennas and Propagation (EuCAP)*, 2781–2785, Mar. 2017.

39. Jilani, S. F., B. Greinke, Y. Hao, and A. Alomainy, "Flexible millimetre-wave frequency reconfigurable antenna for wearable applications in 5G networks," *URSI International Symposium on Electromagnetic Theory (EMTS)*, 846–848, Aug. 2016.

40. Rahimian, A., Y. Alfadhl, and A. Alomainy, "Analytical and numerical evaluations of flexible V-band Rotman lens beamforming network performance for conformal wireless subsystems," *Progress

*In Electromagnetics Research B*, Vol. 71, 77–89, 2016.

41. Vo Dai, T. K. and O. Kilic, "Compact Rotman lens structure configurations to support millimeter wave devices," *Progress In Electromagnetics Research B*, Vol. 71, 91–106, 2016.

42. Clemens, M. and T. Weiland, "Discrete electromagnetism with the finite integration technique," *Progress In Electromagnetics Research*, Vol. 32, 65–87, 2001.

43. Weiland, T., M. Timm, and I. Munteanu, "A practical guide to 3-D simulation," *IEEE Microwave Magazine*, Vol. 9, No. 6, 62–75, Dec. 2008.

44. Attaran, A. and S. Chowdhury, "Fabrication of a 77 GHz Rotman lens on a high resistivity silicon wafer using lift-off process," *International Journal of Antennas and Propagation*, 1–9, article ID: 471935, 2014.